Kinetics of Hydrogen Atom Abstraction from Substrate by an Active Site Thiyl Radical in Ribonucleotide Reductase

JACS
JOURNAL OF THE AMERICAN CHEMICAL SOCIETY

Article

pubs.acs.org/JACS

Kinetics of Hydrogen Atom Abstraction from Substrate by an Active Site Thiyl Radical in Ribonucleotide Reductase

Lisa Olshansky,[†,‡] Arturo A. Pizano,[†] Yifeng Wei,[‡] JoAnne Stubbe,*[,‡] and Daniel G. Nocera*[,†]

[†]Department of Chemistry and Chemical Biology, Harvard University, 12 Oxford Street, Cambridge, Massachusetts 02138, United States

[‡]Department of Chemistry, Massachusetts Institute of Technology, 77 Massachusetts Avenue, Cambridge, Massachusetts 02139, United States

Supporting Information

ABSTRACT: Ribonucleotide reductases (RNRs) catalyze the conversion of nucleotides to deoxynucleotides in all organisms. Active *E. coli* class Ia RNR is an $\alpha_2\beta_2$ complex that undergoes reversible, long-range proton-coupled electron transfer (PCET) over a pathway of redox active amino acids (β-Y_{122} → [β-W_{48}] → β-Y_{356} → α-Y_{731} → α-Y_{730} → α-C_{439}) that spans ∼35 Å. To unmask PCET kinetics from rate-limiting conformational changes, we prepared a photochemical RNR containing a [Re^1] photooxidant site-specifically incorporated at position 355 ([Re]-β_2), adjacent to PCET pathway residue Y_{356} in β. [Re]-β_2 was further modified by replacing Y_{356} with 2,3,5-trifluorotyrosine to enable photochemical generation and spectroscopic observation of chemically competent tyrosyl radical(s). Using transient absorption spectroscopy, we compare the kinetics of Y· decay in the presence of substrate and wt-α_2, Y_{731}F-α_2 ,or C_{439}S-α_2, as well as with 3′-[^{2}H]-substrate and wt-α_2. We find that only in the presence of wt-α_2 and the unlabeled substrate do we observe an enhanced rate of radical decay indicative of forward radical propagation. This observation reveals that cleavage of the 3′-C−H bond of substrate by the transiently formed C_{439}· thiyl radical is rate-limiting in forward PCET through α and has allowed calculation of a lower bound for the rate constant associated with this step of $(1.4 \pm 0.4) \times 10^4$ s^{-1}. Prompting radical propagation with light has enabled observation of PCET events heretofore inaccessible, revealing active site chemistry at the heart of RNR catalysis.

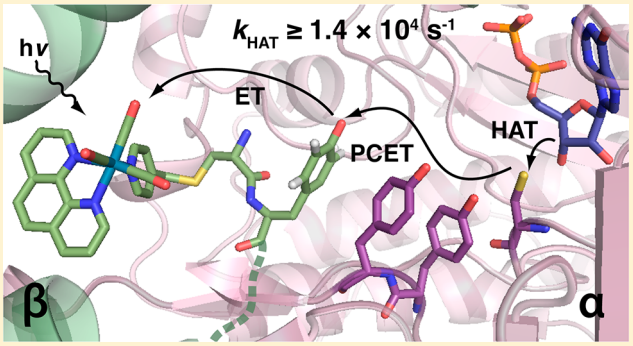

INTRODUCTION

Managing the coupled translocation of protons and electrons is the keystone to energy storage and conversion.[1−5] Biological systems have evolved to capitalize on proton-coupled electron transfer (PCET) to execute energy conversions efficiently and with exquisite control.[6,7] *E. coli* class Ia ribonucleotide reductase (RNR) maintains reversible[8,9] PCET over ∼35 Å[10−13] via a multistep, proton-coupled hopping mechanism and thus serves as a paradigm for the study of PCET in biology.[14,15]

RNR catalyzes the conversion of nucleotides to deoxynucleotides, the bottleneck in de novo production of monomeric DNA building blocks.[16] The active form of *E. coli* class Ia RNR is composed of two homodimeric subunits, α_2 and β_2 (Figure 1a).[13,17] The active site is located in α, while the diferric-Y_{122}· cofactor required to initiate active site chemistry is buried deep within β (Figure 1a). The rate-determining step in turnover consists of a conformational change triggered by substrate binding.[8] This process initiates radical translocation by way of bidirectional PCET to β-Y_{122}· in which a proton is transferred from a specific water molecule ligated to the diferric cluster,[18] while the electron transfer (ET) results in oxidation of β-Y_{356}.[19] β-Y_{356}· then oxidizes α-Y_{731} across the α/β subunit interface which subsequently oxidizes α-Y_{730} and, in turn, α-C_{439} in sequential PCET steps (Figure 1b).[15,20,21] The C_{439}· thiyl radical initiates active site chemistry by abstracting H· from the C3′-position of substrate.[22,23] Multistep active site radical chemistry follows,[16,24] resulting in reoxidation of C_{439} and reverse PCET along the same pathway of redox active amino acid residues to restore the radical resting state at β-Y_{122}·.[8,9]

Despite the fact that this multistep radical transport pathway presents RNR as an ideal system in which to examine biological PCET kinetics, rate-determining conformational changes have largely precluded such studies. In order to disentangle conformational gating from PCET kinetics, we have developed photochemical RNRs.[25] Bypassing conformationally triggered reduction of the Y_{122}· cofactor, we instead initiate PCET events midway through the RNR mechanism by photooxidation of Y_{356} (Figure 1b). Synchronization in this way has enabled detailed studies of photoinitiated substrate turnover,[26] spectroscopic observation of photogenerated radicals,[27] and direct measurement of radical injection rates into α_2.[28] For initial

Received: July 18, 2014
Published: October 29, 2014

   dx.doi.org/10.1021/ja507313w | J. Am. Chem. Soc. 2014, 136, 16210−16216

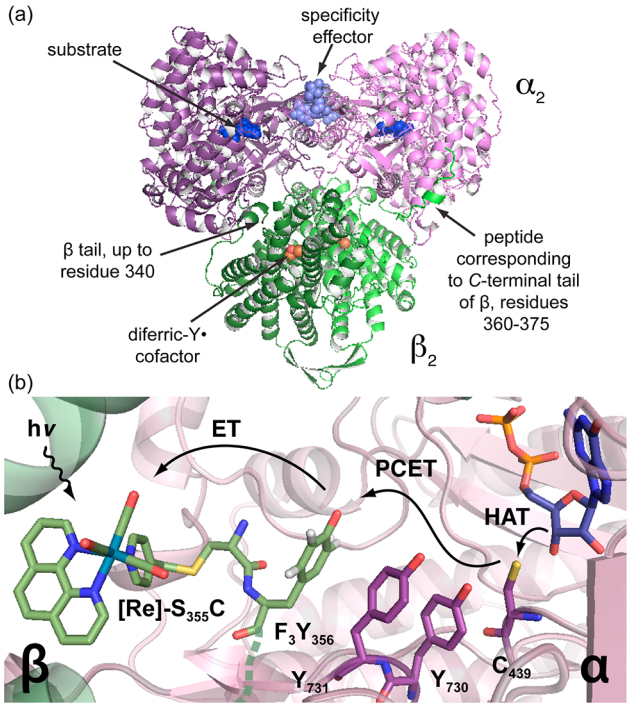

Figure 1. (a) Pseudoatomic model of the active *E. coli* class Ia RNR $\alpha_2\beta_2$ complex[10,13,32] using PDB files 1MXR[33] and 4R1R.[34] α_2 (purple and violet) binds substrate (blue), and effector (slate), and crystallizes with the 20-mer peptide corresponding to the *C*-terminal tail of β. β_2 (forest and light green) contains the μ-O-Fe^{III}_2/Y_{122}· cofactor (Fe, brown; μ-O, red). (b) Illustration of photoinitiated radical transport over the PCET pathway in α (purple), and β (green) via excitation of [Re^I] appended to β-$S_{355}C$ and with 2,3,5-F_3Y replacing β-Y_{356}. Residues 340−360 are disordered in the β_2 structure, and the [Re^I]-C_{355}−F_3Y_{356} fragment (constructed from the [Re^I]-Br crystal structure)[29] is placed in a hypothetical position (dashed green line) intended for illustrative purposes only.

constructs, the β_2 subunit was replaced by a short peptide encompassing the 20 *C*-terminal residues of the β_2 protein. More recently, we have developed a β_2 in which three mutations ($C_{268}S$, $C_{305}S$, and $S_{355}C$) render a single cysteine residue surface-exposed, facilitating site-specific conjugation of a bromomethylpyridyl rhenium(I) tricarbonyl phenanthroline complex to position 355 ([Re^I], Figure 1b).[29] By measuring the [Re^I]* excited-state lifetimes of [Re]-β_2 and [Re]-Y_{356}F-β_2 under different conditions we have shown that this photochemical β_2 is capable of reporting on Y_{356} oxidation.[30] However, attempts to measure radical propagation kinetics directly were prevented by fast charge recombination and thus a low yield of photochemically produced radical.

We have now achieved direct observation of Y· propagation by circumventing the requirement for concomitant proton transfer during the generation of Y_{356}·. Installation of an unnatural 2,3,5-trifluorotyrosine[31] in place of Y_{356} ([Re]-F_3Y_{356}-β_2, Figure 1b) has successfully boosted the yield of the photochemically generated radical, allowing spectroscopic resolution of downstream radical propagation kinetics by transient absorption (TA) spectroscopy. We have shown that this construct is competent for photoinitiated enzymatic turnover and present the first direct measure of Y· propagation kinetics through the active $\alpha_2\beta_2$ RNR complex. By comparing the kinetics of Y· decay in the presence of substrate and wt-α_2, Y_{731}F-α_2, or C_{439}S-α_2, as well as with [3′-^{2}H]-substrate and wt-α_2, we find that only in the presence of wt-α_2 and substrate with natural isotopic abundance are radical decay kinetics enhanced. These data support that cleavage of the 3′-C−H bond of substrate by the transiently formed C_{439}· thiyl radical is rate-limiting in forward PCET through α. We report a lower limit for the rate constant associated with this step of $(1.4 \pm 0.4) \times 10^4$ s^{-1}. Unmasking PCET events in the active $\alpha_2\beta_2$ RNR has provided a first direct measure of active site kinetics in the class Ia enzyme, yielding new evidence for a long-standing model and shedding light on the mechanism by which RNR maintains control and specificity during long-range PCET.

MATERIALS AND METHODS

Materials. Wt-α_2 (2000 nmol/mg/min) was expressed from pET28a-*nrdA* and purified as previously described.[35] Glycerol stocks of Y_{731}F-α_2 and C_{439}S-α_2 were available from a previous study[28] and were expressed and purified as wt-α_2. All α_2 proteins were prereduced prior to use.[21] [5-^{3}H]-cytidine 5′-diphosphate sodium salt hydrate ([5-^{3}H]-CDP) was purchased from ViTrax (Placentia, CA). 3′-Deuterated cytidine 5′-diphosphate ([3′-^{2}H]-CDP) was available from a previous study,[36] in which it was synthesized as reported.[22,23] Tricarbonyl(1,10-phenanthroline)(4-bromomethyl-pyridine)rhenium-(I) hexafluorophosphate ([Re^I]-Br) was available from a previous study.[29] *E. coli* thioredoxin (TR, 40 μmol/min/mg) and thioredoxin reductase (TRR, 1800 μmol/min/mg) were prepared as previously described.[37,38] 2,3,5-Trifluorotyrosine was synthesized enzymatically from pyruvate, ammonia, and 2,3,6-trifluorophenol with tyrosine phenol lyase as the catalyst.[39] Assay buffer consists of 50 mM HEPES, 15 mM $MgSO_4$, and 1 mM EDTA adjusted to the specified pH.

Preparation of [Re]-F_3Y_{356}-β_2. Construction of $C_{268}S/C_{305}S/S_{355}C/Y_{356}Z$-pBAD-*nrdB* was achieved by site-directed mutagenesis using pBAD-*nrdB* as a template, and primers listed in the Supporting Information. *E. coli* TOP10 cells were cotransformed with the newly constructed *nrdB* plasmid and pEVOL-F_nY-aaRS obtained from a previous study,[31] plated on LB-agar plates supplemented with 100 μg/mL ampicillin and 35 μg/mL chloramphenicol and incubated at 37 °C overnight. A 1 mL culture containing the same antibiotics was inoculated with a single colony, incubated at 37 °C for 10 h, and then used to inoculate a small culture grown overnight at 37 °C. This starter-culture was used to inoculate 4 × 2L cultures of 2xYT at a 100-fold dilution. The cells were grown in the presence of 1.5 mM 2,3,5-F_3Y until reaching an OD_{600} of 0.5, at which point the F_nY-aaRS and *nrdB* genes were induced with arabinose (0.05% w/v). The cells were grown for an additional 4 h to a final OD_{600} of ∼1.5 and then harvested by centrifugation (3000 × *g*, 10 min, 4 °C). Yields of ∼2 g/L were obtained. Success of expression was assessed by 10% SDS-PAGE. The protein was purified by anion-exchange chromatography following a previously reported protocol,[40] to give 10−15 mg per g of cell paste. Holo-$S_{355}C$/2,3,5-F_3Y_{356}-β_2 contained 0.6 Y·/β_2 and exhibited no enzymatic activity. This variant is inactive due to the presence of a thiol/thiolate in the tricysteine mutant, which may be oxidized by F_3Y·. This quenching process is not a concern in the photoRNR experiments because conjugation to [Re^I] results in a thioether, which is difficult to oxidize. Purified material contained ≤5% $\beta\beta'$ heterodimer resulting from the presence of protein truncated at position 356 (a consequence of the method used for unnatural amino acid incorporation). Treatment with hydroxyurea to quantitatively reduce Y_{122}·, and labeling with [Re^I]-Br were achieved as reported previously,[29] to yield met-[Re]-F_3Y_{356}-β_2 exhibiting >95% labeling efficiency.

Steady-State Emission pK_a Titration. The steady-state emission intensity of 5 μM [Re]-F_3Y-β_2 in the presence of 1 mM CDP, 3 mM ATP, and 20 μM wt-α_2 was measured in buffer containing 50 mM of either MES (pH 5.2−6.8) or HEPES (pH 7.0−7.6), 15 mM $MgSO_4$, and 1 mM EDTA. Excitation at 315 nm using a 420 nm long-pass cutoff filter allowed spectra to be recorded over 450−650 nm, scanning 3 times per sample at a rate of 0.1 nm/s and detecting in 0.5 nm steps. Samples were held at 25 °C for 2 min prior to scan and

dx.doi.org/10.1021/ja507313w | J. Am. Chem. Soc. 2014, 136, 16210−16216

throughout the duration of the measurement. Integrated emission intensity was plotted versus pH and fit to eq 1 (Figure S1). Here, I corresponds to integrated emission intensity and I_{max} and I_0 correspond to I at pH 7.6 and 5.2, respectively.

$$10^{(pH-pK_a)} = \frac{I - I_0}{I_{max} - I_0} \quad (1)$$

Photochemical Turnover. Single turnover experiments under photochemical conditions were performed by mixing 10 μM each of met-[Re]-F_3Y-β_2 with wt-α_2, $Y_{731}F$-α_2, or $C_{439}S$-α_2 in the presence of 0.2 mM [5-^{3}H]-CDP (specific activity 26,700 cpm/nmol), 1 mM ATP, and 10 mM $Ru(NH_3)_6Cl_3$ in assay buffer at pH 7.6. Samples were placed in a 4 mm × 4 mm quartz cuvette and held at 25 °C under illumination for 10 min with white light powered at 800 W (35 V and 24 A DC) in conjunction with a 313 nm long-pass cutoff filter. Quantitation of radioactive products by scintillation counting and confirmation of product identity (Figure S2) were performed as previously described.[30] Equivalents of dCDP per α_2 produced in the presence of [Re]-F_3Y-β_2 were normalized to dCDP production in the presence of wt-β_2 under the photochemical conditions, which produces 1.2 equiv/α_2 of a theoretical maximum of 4 equiv/α_2. Photochemical activity for 3−6 independent samples was determined, and the standard deviation associated with both wt-β_2 and [Re]-F_3Y-β_2 dCDP production was propagated during normalization.

Nanosecond Laser Flash Photolysis. Samples were prepared in a total volume of 750 μL and recirculated through a 1 cm path length flow cell to reduce sample decomposition. An inline filter (Acrodisc 13 mm 0.2 μM Supor Membrane, Pall Corporation) was used to collect solid photoproducts. Optical long-pass cutoff filters (λ > 375 nm) were used to filter probe light before detection to remove scattered 355 nm pump light. Samples contained 50 μM [Re]-F_3Y-β_2; 75 μM of wt-α_2, $Y_{731}F$-α_2, or $C_{439}S$-α_2; 3 mM ATP; and either 1 or 0.5 mM CDP or [3′-^{2}H]-CDP.

Laser experiments were performed using a system that has previously been described.[28] Single wavelength kinetics data were collected at 412.5 nm using slit widths corresponding to 0.7 nm resolution and recorded over 1000 laser shots for each sample. TA spectra were collected over 500 four-spectrum sequences where two of four conditions result in exposure to the pump beam.

Lifetimes were obtained by averaging three sets of decay traces from three unique samples of a single protein preparation (both wt-α_2 and [Re]-F_3Y-β_2; expression, purification, and [Re]-labeling) (Trial 1 in Table S1), according to eq 2:

$$y = y_0 + Ae^{-x/\tau} \quad (2)$$

Lifetimes from the decay traces for another three sets of unique samples were then obtained using a second protein preparation (Trial 2 in Table S1). Table 1 lists the propagated error for the six measurements across the two trials with weighted averages derived from error associated with the fit for each data set within a trial, compounded with the standard deviation between the two trials. An exemplary data set, along with fits to eq 2, and associated residuals analysis are included in Figure S3.

Table 1. Y· Lifetimes for α_2-Variant/Substrate Combinations

α_2-variant	substrate	$\tau/\mu s^a$
wt	CDP	18 (1)
$Y_{731}F$	CDP	24 (1)
$C_{439}S$	CDP	25 (2)
wt	[3′-^{2}H]-CDP	26 (1)

[a]Photogenerated Y· lifetimes monitored by TA spectroscopy at 412.5 nm and fit to monoexponential decay from 3 to 76.5 μs (Figure S3). Weighted averages represent duplicate sets of three measurements each, on two separate protein preparations of [Re]-F_3Y-β_2 and wt-α_2. Samples contain 50 μM met-[Re]-F_3Y-β_2, 75 μM α_2 variant, 1 mM or 0.5 mM CDP or [3′-^{2}H]-CDP, 3 mM ATP, 10 mM $Ru(NH_3)_6Cl_3$, and assay buffer at pH 8.2.

RESULTS

pK_a of 2,3,5-F_3Y_{356} within the $\alpha_2\beta_2$ Complex. Photochemical generation of an observable population of F_3Y_{356}· is enhanced when the amino acid resides in its deprotonated state. This enhanced radical generation is a direct consequence of the ability to generate the radical by removal of only an electron as opposed to removal of an electron and proton (i.e., PCET). To determine the optimum pH for photochemical radical generation, we measured the pK_a of F_3Y_{356} within the α_2/[Re]-β_2 complex. This measurement was accomplished by monitoring the steady-state emission from the rhenium complex excited state ([Re^I]*), which is quenched much more effectively when the adjacent F_3Y is deprotonated.[41] Plotting emission intensity as a function of pH revealed a pK_a of 6.2 ± 0.1 (Figure S1). This value is in line with the pK_a of 6.4 measured for the free amino acid derivative,[42] particularly in light of the fact that a positively charged [Re^I] complex is present. The pK_a measured here is also in line with the value of 6.8 predicted by titrations using 3-NO_2Y_{356}-β_2, in which, by comparison with free NO_2Y, the ΔpK_a due to perturbations arising from the protein environment at position 356 was inferred.[40] All subsequent spectroscopy was conducted at pH 8.2 such that ∼99% of F_3Y_{356} is deprotonated.

Observation of Transient Y·. In order to observe photogenerated Y·'s, charge recombination within the initially formed charge-separated state ([Re^0]-F_3Y_{356}·-β_2) must be prevented. Therefore, we applied flash-quench methodology by including an excess of $Ru(NH_3)_6Cl_3$ in reaction mixtures. Bimolecular quenching of the [Re^I]* excited state furnishes the [Re^{II}] complex via reduction of $Ru(NH_3)_6^{3+}$ to $Ru(NH_3)_6^{2+}$. This [Re^{II}] species is capable of driving rapid oxidation of trifluorotyrosinate (Figure 2a). Figure 2b shows the TA spectrum of Y· collected 3 μs after excitation, at which point nearly all photochemistry is completed and F_3Y· and/or Y· are the only transient species contributing to the absorption feature centered at 412 nm. The overall photochemical yield of Y· is ∼1.9% (calculation included in the Supporting Information). Experiments were performed at protein concentrations such that >97% of [Re]-F_3Y_{356}-β_2 is complexed to α_2 (based on the previously reported K_D of 0.7 ± 0.1 μM, measured for [Re]-β_2 binding to α_2 under the same conditions).[30] The control experiment performed with [Re]-$Y_{356}F$-β_2 (black, Figure 2b) shows a minor TA signal, which we have previously observed and ascribed to off-pathway generation of Y·.[30] In the absence of an adjacent redox active amino acid, off-pathway radical generation is maximized. Thus, this spectrum (black, Figure 2b) represents a maximum possible contribution to the observed signal and is likely greater than any off-pathway contributions operative when F_3Y or Y is present.

Photochemical Competence for Turnover. To evaluate the relevance of photochemically generated Y· in RNR chemistry, we sought to verify chemical competence for enzymatic turnover via photochemical initiation. Steady-state illumination under single turnover conditions in the presence of radiolabeled substrate ([5-^{3}H]-CDP), effector (ATP), $Ru(NH_3)_6Cl_3$, and α_2 allows quantitation and identification of photogenerated products.[30,41,43] Of note, the μ-O-Fe^{III}_2/Y_{122}· cofactor of [Re]-F_3Y_{356}-β_2 has been reduced with inhibitor hydroxyurea to form met-[Re]-F_3Y_{356}-β_2; thus the normal mechanism for turnover is not viable with this construct.

dx.doi.org/10.1021/ja507313w | J. Am. Chem. Soc. 2014, 136, 16210−16216

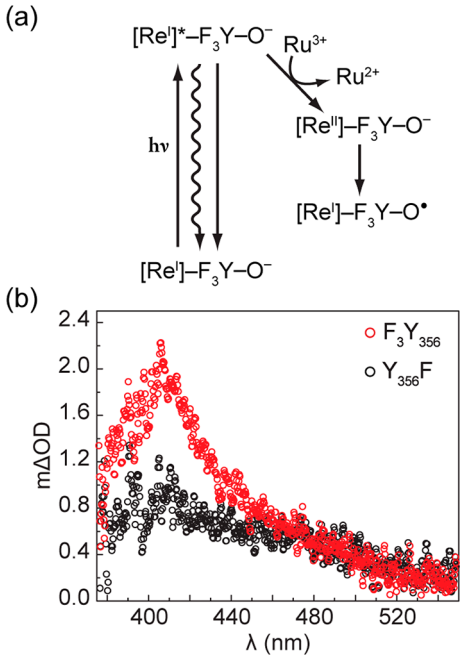

Figure 2. (a) Scheme describing the photochemistry of $F_3Y\cdot$ generation; (b) TA spectra collected 3 μs after 355 nm excitation of 50 μM [Re]-F_3Y_{356}-β_2 (red) or [Re]-$Y_{356}F$-β_2 (black), and 75 μM α_2, 1 mM CDP, 3 mM ATP, and 10 mM $Ru(NH_3)_6Cl_3$, in assay buffer at pH 8.2.

Photochemical production of dCDP is 9 ± 4% that of wt-β_2 under identical conditions (Figures 3 and S2), which produces 1.2 dCDP/α_2 out of a theoretical maximum of 4. Dark controls and reactions with $Y_{731}F$-α_2 and $C_{439}S$-α_2 variants produce negligible amounts of product.

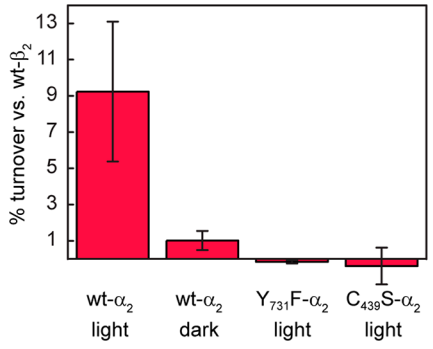

Figure 3. Photochemical turnover of met-[Re]-F_3Y_{356}-β_2 (10 μM), [5-^{3}H]-CDP (0.2 mM), ATP (3 mM), $Ru(NH_3)_6Cl_3$ (10 mM), and wt-, $Y_{731}F$-, or $C_{439}S$-α_2 (10 μM) in assay buffer, pH 7.6 at 25 °C. Numbers are presented as a percentage of product observed with wt-β_2. Error bars represent 1 standard deviation for 3–6 independent trials.

Pathway and Isotope Dependence of Y· Lifetime. We set out to explore individual PCET steps by measuring the kinetic behavior of Y· under different conditions. We compared the lifetime of transiently formed Y· (τ) in the presence of CDP, ATP, and wt-α_2 with that of τ in the presence of CDP, ATP, and α-variants containing redox-inactive pathway substitutions, as well as in the presence of [3′-^{2}H]-CDP, ATP, and wt-α_2. Lifetime data were determined from measurements of three unique samples from a single protein preparation of both wt-α_2 and [Re]-F_3Y-β_2; data sets from two protein preparations were measured. Accordingly, the data in Table 1 are the propagated error for the six measurements across the two trials. Of note, the initiation process in which $F_3Y_{356}^-$ is oxidized by [Re^{II}] simply generates the radical on the PCET pathway. All fits to kinetics data begin at 3 μs, after the $F_3Y\cdot$ has formed. Thus, by removing the proton dependence of the initiation step, we are able to increase the yield of the radical (by relying only on an ET vs PCET for radical initiation), and we do not alter the PCET mechanism at play during the steps of interest that follow. With the exception of τ measured in the presence of $Y_{731}F$-α_2, the lifetime in each case corresponds to a total signal composed of contributions from $F_3Y_{356}\cdot$ in β, $Y_{731}\cdot$ and $Y_{730}\cdot$ in α_2. Similar signal amplitudes were observed at t = 0 within each trial (Table S1), revealing that Y· generation was similar to the different α_2 variants and substrates.

We found that the measured lifetime of τ = 18 ± 1 μs for wt-α_2 is extended to 24 ± 1 μs for the $Y_{731}F$-α_2 variant, which cannot produce a radical in α_2 (Table 1). This observation suggests that the PCET pathway in α introduces an additional route for Y· decay. The significant difference between these two values provides a means of differentiating on- and off-pathway radical decay. The relative kinetics of the productive, on-pathway contribution to the total decay is calculated according to eq 3, where τ_o represents the lifetime measured in the presence of $Y_{731}F$-α_2. The resultant rate constant (k_{obs}) is (1.4 ± 0.4) × 10^4 s^{-1}.

$$k_{obs} = \frac{1}{\tau} - \frac{1}{\tau_0} \quad (3)$$

In order to understand which processes in α limit the rate of radical transport, we next blocked the interior end of the PCET pathway by using $C_{439}S$-α_2. A lifetime identical to that measured in the presence of $Y_{731}F$-α_2 was observed (Table 1), revealing that the rate-determining step operative in the presence of wt-α_2 occurs either during or after oxidation of residue C_{439}. We note, however, that this observation does not reveal whether or not radical injection into the α subunit occurs in the presence of this variant. It could be envisioned that the downstream perturbation to the PCET pathway imposed by the $C_{439}S$ amino acid substitution precludes radical injection entirely. Thus, either radical injection followed by rapid reverse PCET and quenching occurs or injection is precluded. Both possibilities provide evidence for strict conformational control over PCET events. Throughout our analysis we have assumed that, in the presence of wt-α_2 and CDP, new routes for off-pathway Y· decay have not been introduced. In all cases, τ_o is unrestricted in its definition and simply represents the Y· lifetime via any avenue of nonproductive decay. Thus, in calculating k_{obs} we apply the same τ_o value for nonproductive decay in the case where the productive pathway (turnover) has also been enabled.

Once C_{439} is oxidized, the ensuing radical abstracts a hydrogen atom from the 3′-position of substrate (Scheme 1). Subsequent loss of a molecule of water from the 2′-position represents the first irreversible step of turnover. This irreversibility renders any subsequent steps inconsequential to the Y· decay rate. Thus, the rate-determining step with respect to Y· decay in our system (namely, where the native pathway through β is overridden) must be either oxidation of C_{439} or H· abstraction from C3′ of substrate. To differentiate between these two possibilities we next measured τ in the presence of

dx.doi.org/10.1021/ja507313w | J. Am. Chem. Soc. 2014, 136, 16210–16216

Scheme 1. Mechanistic Model Describing Y· Decay

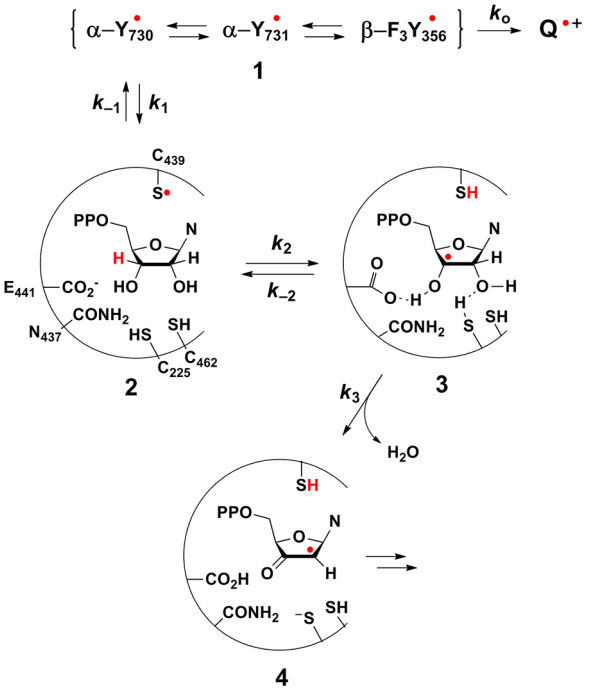

wt-α_2 and [3′-^{2}H]-CDP. Here, a lifetime similar to that observed in the presence of wt-α_2 and CDP would suggest that oxidation of C_{439} by Y_{730}· is rate-determining, because slowing down the subsequent step has no effect on τ. Alternatively, a lifetime intermediate between that observed in the presence of wt-α_2 and CDP and that observed in the presence of pathway-blocked variants would indicate that cleavage of the 3′-C–H bond by C_{439}· is rate-limiting. We found that the latter case prevails, and to its extreme extent.

Introduction of deuterium at the 3′-position of substrate completely alters the relative kinetics of the system, resulting in τ statistically identical to τ_o (Table 1). Further, unlike in the case with C_{439}S-α_2, here we are using wt-α_2 and so no perturbation to the PCET pathway is incurred. Therefore, in this case we do assume that radical injection into α occurs. Observation of this isotope effect (IE) suggests that we have successfully uncoupled radical translocation from conformational gating, thus allowing for the first direct measure of PCET kinetics within the $\alpha_2\beta_2$ complex.

DISCUSSION

More than 30 years ago [3′-^{3}H]-NDPs were used to investigate the mechanism of RNR.[22,23] Small amounts of RNR-mediated ^3H_2O release and $^T[V/K]$ isotope effects provided strong evidence that 3′-C–H bond cleavage occurs during NDP reduction. This study also established that the first irreversible step during a single turnover occurs after hydrogen atom abstraction from substrate and formed the underpinning for the mechanistic model shown in Scheme 1 (intermediates **2**–**4**) and Figure S4.

Stepwise PCET between Tyr-O· → Cys-S· → R_3C· akin to the interconversion of **1** → **2** → **3** in Scheme 1 seems contrary to thermodynamic favor (bond dissociation energies of PhO–H, RS–H, and $HOCH_2$–H are ∼86, 91, and 94 kcal/mol, respectively).[16,44,45] However, a central tenet of the model proposed in Scheme 1 is that enzymatic coupling of endergonic steps to an irreversible reaction can provide a means of overcoming thermodynamic hurdles. The irreversible and entropically favored release of a molecule of water from the 2′-position of substrate (e.g., **3** → **4** in Scheme 1) is postulated to drive the RNR reaction forward as and when small amounts of intermediate **3** are formed from the reversible steps leading up to it. The loss of a rate enhancement for Y· decay in the presence of [3′-^{2}H]-CDP reveals a primary IE on the cleavage of the substrate 3′-C–H bond, providing direct evidence in support of this model.

The steps in the RNR mechanism that are relevant to the current experiment are outlined in Scheme 1. We note that radical translocation in our system is initiated midstream along the PCET pathway; thus steps within the β subunit are inconsequential. Here, **1** accounts for our experimental observable, a composite signal of unknown relative contributions from F_3Y_{356}· in β, Y_{731}· and Y_{730}· in α_2. Reoxidation of $F_3Y_{356}^-$ by Y_{731}· is predicted to be ∼110 mV uphill at pH 8.2 based on the relative potentials of these amino acids in solution.[42] Yet, experiments in RNR suggests that Y_{356} is ∼100 mV easier to oxidize than Y_{731} within the subunit interface.[46] Similarly, Y_{731}· and Y_{730}· have been predicted,[47] and experimentally shown,[46] to be isoenergetic within the enzyme complex. Thus, all of these radical species have been drawn as reversibly interconverting and reduction of intermediate **1** by an off-pathway quencher, **Q**, can potentially occur by way of any of these radical intermediates.

On-pathway Y· decay occurs by oxidation of C_{439} to give intermediate **2**. Upon oxidation, C_{439}· reversibly abstracts H· from the 3′-position of substrate to generate **3**. General base (E_{441}) and acid (C_{225}) catalysis facilitate dehydration from the 2′-position to yield the 2′-α-ketyl radical intermediate (**4**). Despite the fact that active site chemical transformations following the formation of **4** ultimately result in the regeneration of the C_{439}· and reverse PCET to reform **1** (Figure S4),[48] these processes occur on a much slower time scale (∼100 s^{-1}) than under examination here.[49] Accordingly, **1** is not expected to reform during the time course of the experiment. Thus, **4** represents a terminal product with respect to Y· decay and the mechanistic steps relevant to our experimental conditions are limited to the interconversion of species **1**–**4** in Scheme 1.

Our results comparing τ in the presence of [3′-^{2}H]-CDP versus CDP reveal that the rate enhancement for nonlabeled CDP occurs after oxidation of C_{439}. However, the implications of the reversibility of the oxidation of C_{439} on the radical lifetimes of **1** must be considered. With little kinetic information regarding the equilibrium between **1** and **2**, we turn to small molecule model studies in which the kinetics of bimolecular oxidation of Cys by Tyr· were examined by pulse radiolysis.[50] These studies report a rate constant of 2×10^6 M^{-1} s^{-1} and that the reverse reaction (oxidation of Tyr by Cys·) is significantly faster.[50] These results suggest that a pre-equilibrium may be established between intermediates **1** and **2** in our system and facilitates an estimate for the magnitude of the corresponding equilibrium constant, $K_{\pm1}$ (k_1/k_{-1}), from thermodynamic values. Electrochemical measurements of tyrosine and glutathione reveal that cysteine and tyrosine have approximately equal midpoint potentials at pH 7.0 (0.94 ± 0.04 V and 0.93 ± 0.02 V, respectively).[51] However, calculations based on a trapped form of the active RNR complex suggest that oxidation of C_{439} by Y_{730}· is endergonic by 3–4 kcal/mol, resulting in $K_{\pm1} \approx 10^{-2}$.[47] Taken together, these

dx.doi.org/10.1021/ja507313w | J. Am. Chem. Soc. 2014, 136, 16210–16216

studies support that **2** is formed reversibly from **1** and that the resultant equilibrium constant is ≤1. We note that **2** has never been observed or trapped in a class I enzyme, indicating that this intermediate is likely consumed upon its formation. This scenario renders k_{obs} a lower bound for k_2 where the extent to which the actual k_2 is greater than k_{obs} increases as $K_{\pm 1}$ decreases from unity.

The reversibility of H atom abstraction may also lead to a case where k_2 is greater than k_{obs}. The extent to which this is manifest depends upon the efficiency with which **3** proceeds forward as a fraction of its total decay. This efficiency can be described by a net rate constant equal to $k_3/(k_{-2} + k_3)$, which has a maximum value of 1. Reactions similar to both of the processes described by k_{-2} and k_3 have been studied extensively, producing rate constants ranging from 10^6-10^8 M^{-1} s^{-1},[52−56] and 10^6-10^8 s^{-1},[57−59] for k_{-2} and k_3, respectively. Though it is difficult to compare bimolecular reactions in solution to those within an enzyme active site, we note that these values are all 10^2-10^4-fold faster than the corresponding bimolecular rate constants akin to conversion of **2** → **3** (k_2).[52−56] Applying the limiting values from these model studies, we find that, at the highest enzymatic efficiency, a factor of 1 is obtained for $k_3/(k_{-2} + k_3)$ and thus the reversibility of H· abstraction does not affect k_{obs}. At the lowest enzymatic efficiency, $k_3/(k_{-2} + k_3)$ is calculated to be 10^{-2}, rendering k_2 10^2-fold greater than k_{obs}.

In light of the preceding discussion, it is clear that the k_{obs} reported here (1.4×10^4 s^{-1}) is a lower limit for thiyl radical mediated H· abstraction from C3′ of substrate. Chemical precedent for C−H bond cleavage by thiyl radicals has been established by a number of methods including pulse radiolysis,[52−56] laser flash photolysis,[60] and NMR[61] and EPR[62] competition experiments. Rate constants for C−H bond cleavage in deoxyribose, tetrahydrofuran, 2-propanol, glucose, and other 2° alcohols and ethers by cysteine, glutathione, and pennicilamine thiyl radicals have been measured by pulse radiolysis to give second-order rate constants in the range $(1.2-1.8) \times 10^4$ M^{-1} s^{-1}.[52−56] These studies bolster our interpretation that hydrogen atom transfer from C3′ to C_{439}· is rate-limiting within the context of Scheme 1 and provide values that are consistent with the rate constant reported here.

Previous success in unmasking radical translocation kinetics in RNR is limited to only three examples. Replacing β-Y_{122} with NO_2Y, whose high reduction potential and low pK_a decouple PT from ET, allowed examination of β-NO_2Y_{122}· reduction by stopped-flow absorption and rapid freeze quench EPR spectroscopies.[49] This work, though still limited by mixing times and possibly by further conformational gating, allowed the rate constant for ET to NO_2Y_{122}· (to form NO_2Y^-) to be bracketed with a lower limit of 300 s^{-1}.[49] The limitations imposed by mixing times are completely eliminated with photoRNRs. Modification of the *C*-terminal tail of β with an appended [Re^I]-2,3,6-F_3Y revealed a rate constant of $(3 \pm 2) \times 10^5$ s^{-1} for radical injection into α_2,[28] and this observation was further corroborated by our measurement of the rate constant for charge separation (k_{CS}) in a photo-β_2 containing the native Y residue at position 356 of β, where a $k_{CS} = (4.1 \pm 0.1) \times 10^5$ s^{-1} in the presence of wt-α_2, CDP, and ATP was observed.[30] All of these results are in line with the conclusions presented here: radical injection into the α_2 subunit is faster than subsequent PCET and substrate activation steps.

The fact that C−H bond cleavage from substrate by the transiently formed C_{439}· occurs at 10^4 s^{-1}, along with previous results,[28,30,49] reveals that PCET events occur rapidly during radical translocation. Together with recent findings that implicate alignment of the PCET pathway as a target of conformational gating,[13,18,47] these results suggest that the reaction profile of the active $\alpha_2\beta_2$ complex remains locked in place as radical translocation and subsequent active site chemical steps transpire. This ability to lock the PCET pathway indicates that RNR capitalizes on the constraints imposed by PT distances in achieving acute control over long-range ET.

A number of studies indicate that the PCET pathway of RNR runs slightly thermodynamically uphill in the forward direction,[14,15,31,46,49] and active site chemistry is driven forward by the rapid and irreversible loss of water from the 2′-position of substrate.[24,57−59] This reaction landscape presents a mechanism by which RNR avoids the buildup of reactive amino acid radical intermediates over the course of its ∼70 Å round-trip traverse between α and β. Our observation that HAT from C3′ of substrate to C_{439}· is rate-limiting in forward PCET through α provides further evidence that an uphill PCET pathway generates the initial substrate radical.

■ CONCLUSIONS

Jump-starting radical propagation with light has enabled the direct observation of PCET events previously inaccessible, revealing active site chemistry at the heart of RNR catalysis. Despite the fact that RNR turnover is rate-limited by conformational changes occurring at ∼2−10 s^{-1},[8] radical propagation steps are rapid. To unmask PCET events we have constructed a photochemically competent β_2 subunit capable of generating observable transient Y· species within the $\alpha_2\beta_2$ complex. With this construct, we have observed an IE on cleavage of the substrate 3′-C−H bond, revealing that this step is rate-limiting with respect to Y· propagation through α and allowing us to report a lower bound for the rate constant associated with this step of $(1.4 \pm 0.4) \times 10^4$ s^{-1}. Unmasking PCET events in the active $\alpha_2\beta_2$ RNR has provided a first measure of active site kinetics in the class Ia enzyme, yielding new evidence for a long-standing model and shedding light on the mechanism by which RNR maintains control and specificity during long-range radical transport.

■ ASSOCIATED CONTENT

Supporting Information

Experimental methods and instrumentation; calculation of photochemical Y· yield; complete table of data including τ and ΔOD amplitudes for two trials; pK_a titration; HPLC analysis of radiolabeled photoproducts; single wavelength kinetics data, fitting, and residuals analysis; scheme depicting the entire model for RNR-mediated substrate turnover. This material is available free of charge via the Internet at http://pubs.acs.org.

■ AUTHOR INFORMATION

Corresponding Authors

dnocera@fas.harvard.edu (D.G.N.)
stubbe@mit.edu (J.S.)

Notes

The authors declare no competing financial interest.

■ ACKNOWLEDGMENTS

The authors gratefully acknowledge the NIH for funding (GM 47274 D.G.N., GM 29595 J.S.). L.O. acknowledges the NSF for a graduate fellowship.

■ REFERENCES

(1) Cukier, R. I.; Nocera, D. G. *Annu. Rev. Phys. Chem.* **1998**, *49*, 337−369.
(2) Huynh, M.-H. V.; Meyer, T. J. *Chem. Rev.* **2007**, *107*, 5004−5064.
(3) Hammes-Schiffer, S. *Acc. Chem. Res.* **2009**, *42*, 1881−1889.
(4) Cook, T. R.; Dogutan, D. K.; Reece, S. Y.; Surendranath, Y.; Teets, T. S.; Nocera, D. G. *Chem. Rev.* **2010**, *110*, 6474−6502.
(5) Nocera, D. G. *Inorg. Chem.* **2009**, *48*, 10001−10007.
(6) Dempsey, J. L.; Winkler, J. R.; Gray, H. B. *Chem. Rev.* **2010**, *110*, 7024−7039.
(7) Reece, S. Y.; Nocera, D. G. *Annu. Rev. Biochem.* **2009**, *78*, 673−699.
(8) Ge, J.; Yu, G.; Ator, M. A.; Stubbe, J. *Biochemistry* **2003**, *42*, 10071−10083.
(9) Seyedsayamdost, M. R.; Stubbe, J. *J. Am. Chem. Soc.* **2007**, *129*, 2226−2227.
(10) Uhlin, U.; Eklund, H. *Nature* **1994**, *370*, 533−539.
(11) Bennati, M.; Robblee, J. H.; Mugnaini, V.; Stubbe, J.; Freed, J. H.; Borbat, P. *J. Am. Chem. Soc.* **2005**, *127*, 15014−15015.
(12) Seyedsayamdost, M. R.; Chan, C. T. Y.; Mugnaini, V.; Stubbe, J.; Bennati, M. *J. Am. Chem. Soc.* **2007**, *129*, 15748−15749.
(13) Minnihan, E. C.; Ando, N.; Brignole, E. J.; Olshansky, L.; Chittuluru, J.; Asturias, F. J.; Drennan, C. L.; Nocera, D. G.; Stubbe, J. *Proc. Natl. Acad. Sci. U.S.A.* **2013**, *110*, 3835−3840.
(14) Stubbe, J.; Nocera, D. G.; Yee, C. S.; Chang, M. C. Y. *Chem. Rev.* **2003**, *103*, 2167−2202.
(15) Minnihan, E. C.; Nocera, D. G.; Stubbe, J. *Acc. Chem. Res.* **2013**, *46*, 2524−2535.
(16) Stubbe, J.; van der Donk, W. A. *Chem. Rev.* **1998**, *98*, 705−762.
(17) Brown, N. C.; Reichard, P. *J. Mol. Biol.* **1969**, 25−38.
(18) Wörsdörfer, B.; Conner, D. A.; Yokoyama, K.; Livada, J.; Seyedseyamdost, M. R.; Jiang, W.; Silakov, A.; Stubbe, J.; Bollinger, J. M., Jr.; Krebs, C. *J. Am. Chem. Soc.* **2013**, *135*, 8585−8593.
(19) Seyedsayamdost, M. R.; Stubbe, J. *J. Am. Chem. Soc.* **2006**, *128*, 2522−2523.
(20) Seyedsayamdost, M. R.; Stubbe, J. *J. Am. Chem. Soc.* **2006**, *128*, 2522−2523.
(21) Seyedsayamdost, M. R.; Xie, J.; Cham, C. T. Y.; Schultz, P. G.; Stubbe, J. *J. Am. Chem. Soc.* **2007**, *129*, 15060−15071.
(22) Stubbe, J.; Ackles, D. *J. Biol. Chem.* **1980**, *255*, 8027−8030.
(23) Stubbe, J.; Ator, M.; Krenitsky, T. *J. Biol. Chem.* **1983**, *258*, 1625−1630.
(24) Licht, S.; Stubbe, J. *Compr. Nat. Prod. Chem.* **1999**, *5*, 163−203.
(25) Chang, M. C. Y.; Yee, C. S.; Stubbe, J.; Nocera, D. G. *Proc. Natl. Acad. Sci. U.S.A.* **2004**, *101*, 6882−6887.
(26) Reece, S. Y.; Seyedsayamdost, M. R.; Stubbe, J.; Nocera, D. G. *J. Am. Chem. Soc.* **2007**, *129*, 8500−8509.
(27) Reece, S. Y.; Seyedsayamdost, M. R.; Stubbe, J.; Nocera, D. G. *J. Am. Chem. Soc.* **2007**, *129*, 13828−13830.
(28) Holder, P. G.; Pizano, A. A.; Anderson, B. L.; Stubbe, J.; Nocera, D. G. *J. Am. Chem. Soc.* **2012**, *134*, 1172−1180.
(29) Pizano, A. A.; Lutterman, D. A.; Holder, P. G.; Teets, T. S.; Stubbe, J.; Nocera, D. G. *Proc. Natl. Acad. Sci. U.S.A.* **2012**, *109*, 39−43.
(30) Pizano, A. A.; Olshansky, L.; Holder, P. G.; Stubbe, J.; Nocera, D. G. *J. Am. Chem. Soc.* **2013**, *135*, 13250−13253.
(31) Minnihan, E. C.; Young, D. D.; Schultz, P. G.; Stubbe, J. *J. Am. Chem. Soc.* **2011**, *133*, 15942−15945.
(32) Ando, N.; Brignole, E. J.; Zimanyi, C. M.; Funk, M. A.; Yokoyama, K.; Asturias, F. J.; Stubbe, J.; Drennan, C. L. *Proc. Natl. Acad. Sci. U.S.A.* **2011**, *108*, 21046−21051.
(33) Högbom, M.; Galander, M.; Andersson, M.; Kolberg, M.; Hofbauer, W.; Lassmann, G.; Nordlund, P.; Lendzian, F. *Proc. Natl. Acad. Sci. U.S.A.* **2003**, *100*, 3209−3214.
(34) Eriksson, M.; Uhlin, U.; Ramaswamy, S.; Ekberg, M.; Regnström, K.; Sjöberg, B.-M.; Eklund, H. *Structure* **1997**, *5*, 1077−1092.
(35) Minnihan, E. C.; Seyedsayamdost, M. R.; Uhlin, U.; Stubbe, J. *J. Am. Chem. Soc.* **2011**, *133*, 9430−9440.
(36) Minnihan, E. C., Ph.D. Thesis, Massachusetts Institute of Technology, 2012.
(37) Pigiet, V. P.; Conley, R. R. *J. Biol. Chem.* **1977**, *252*, 6367−6372.
(38) Lunn, C. A.; Kathju, S.; Wallace, B. J.; Kushner, S. R.; Pigiet, V. *J. Biol. Chem.* **1984**, *259*, 10469−10474.
(39) Chen, H.; Gollnick, P.; Phillips, R. S. *Eur. J. Biochem.* **1995**, *229*, 540−549.
(40) Yokoyama, K.; Uhlin, U.; Stubbe, J. *J. Am. Chem. Soc.* **2010**, *132*, 8385−8397.
(41) Reece, S. Y.; Lutterman, D. A.; Seyedsayamdost, M. R.; Stubbe, J.; Nocera, D. G. *Biochemistry* **2009**, *48*, 5832−5838.
(42) Seyedsayamdost, M. R.; Reece, S. Y.; Nocera, D. G.; Stubbe, J. *J. Am. Chem. Soc.* **2006**, *128*, 1569−1579.
(43) Steeper, J. R.; Steuart, C. D. *Anal. Biochem.* **1970**, *34*, 123−130.
(44) Benson, S. W. *Chem. Rev.* **1978**, *78*, 23−35.
(45) McMillen, D. F.; Golden, D. M. *Annu. Rev. Phys. Chem.* **1982**, *33*, 493−532.
(46) Yokoyama, K.; Smith, A. A.; Corzilius, B.; Griffin, R. G.; Stubbe, J. *J. Am. Chem. Soc.* **2011**, *133*, 18420−18432.
(47) Argirević, T.; Riplinger, C.; Stubbe, J.; Neese, F.; Bennati, M. *J. Am. Chem. Soc.* **2012**, *134*, 17661−17670.
(48) Lawrence, C. C.; Bennati, M.; Obias, H. V.; Bar, G.; Griffin, R. G.; Stubbe, J. *Proc. Natl. Acad. Sci. U.S.A.* **1999**, *96*, 8979−8984.
(49) Yokoyama, K.; Uhlin, U.; Stubbe, J. *J. Am. Chem. Soc.* **2010**, *132*, 15368−15379.
(50) Folkes, L. K.; Trujillo, M.; Bartesaghi, S.; Radi, R.; Wardman, P. *Arch. Biochem. Biophys.* **2011**, *506*, 242−249.
(51) Madej, E.; Wardman, P. *Arch. Biochem. Biophys.* **2007**, *462*, 94−102.
(52) Sonntag, C.; Schöneich, C.; Bonifačić, M.; Dillinger, U.; Asmus, K.-D.; Dunster, C.; Willson, R. L.; Prütz, W. A. In *Sulfur-Centered Reactive Intermediates in Chemistry and Biology*; Catgilialoglu, C., Asum, K.-D., Eds.; Plenum Press: New York, 1990; Vol. *A*, series 197, pp 359−399.
(53) Schöneich, C.; Bonifacic, M.; Asmus, K.-D. *Free Radic. Res. Commun.* **1989**, *6*, 393−405.
(54) Pogocki, D.; Schöneich, C. *Free Radic. Biol. Med.* **2001**, *31*, 98−107.
(55) Schöneich, C.; Asmus, K.-D.; Bonifačić. *J. Chem. Soc., Faraday Trans.* **1995**, *91*, 1923−1930.
(56) Tamba, M.; Quintiliani, M. *Radiat. Phys. Chem.* **1984**, *23*, 259−263.
(57) Steenken, S.; Davies, M. J.; Gilbert, B. C. *J. Chem. Soc., Perkin. Trans.* **1986**, *2*, 1003−1010.
(58) Bansal, K. M.; Grätzel, M.; Henglein, A.; Janata, E. *J. Phys. Chem.* **1973**, *77*, 16−19.
(59) Lenz, R.; Giese, B. *J. Am. Chem. Soc.* **1997**, *119*, 2784−2794.
(60) Nauser, T.; Casi, G.; Koppenol, W. H.; Schöneich, C. *J. Phys. Chem. B* **2008**, *112*, 15034−15044.
(61) Nauser, T.; Schöneich, C. *J. Am. Chem. Soc.* **2003**, *125*, 2042−2043.
(62) Mason, R. P.; Rao, D. N. R. *Sulfur-Centered Reactive Intermediates in Chemistry and Biology*; Catgilialoglu, C., Asum, K.-D., Plenum Press: New York, 1990; Vol. *A*, series 197, pp 401−408.